Black Sea Journal of Engineering and Science
doi: 10.34248/bsengineering.1804471

Open Access Journal
e-ISSN: 2619 – 8991

Research Article
Volume 9 - Issue 1: 254-264 / January 2026

FUNCTIONALLY GRADED GRAPHENE NANOPLATELET REINFORCED COMPOSITE NONLINEAR BEAMS

Reha ARTAN[1], İsmail Önder KARTAL[1]*

[1]*Istanbul Technical University, Department of Civil Engineering, 34467, Istanbul, Türkiye*

Abstract: In this study, nonlinear bending behavior of functionally graded graphene nanoplatelet reinforced composite beams is analyzed using Touratier's higher-order shear deformation theory. Nonlinear equilibrium equations and boundary conditions are derived from the minimum potential energy principle and numerically solved. Equilibrium equations are valid for any beam theory. Equilibrium equations of other beam theories can be easily obtained by changing the f(z) function in these equations. The bending, vibration, and buckling of beams can be easily studied by other theories using the given equilibrium equations and boundary conditions. The graphs of all the unknowns of the problem were presented along the length of the beam. In addition, polynomials fitted to the dimensionless numerical results obtained were given.

Keywords: Functionally graded material, Graphene nanoplatelet, Composite beam, Touratier theory, Nonlinear bending, Energy method.

***Corresponding author:** Istanbul Technical University, Department of Civil Engineering, 34467, Istanbul, Türkiye
E mail: kartalism@itu.edu.tr (İ. Ö. KARTAL)
İsmail Önder KARTAL https://orcid.org/0009-0002-0869-023X
Reha ARTAN https://orcid.org/0000-0002-1518-029X

Received: October 15, 2025
Accepted: December 17, 2025
Published: January 15, 2026

Cite as: Artan, R., & Kartal, İ. Ö. (2025). Functionally graded graphene nanoplatelet reinforced composite nonlinear beams. *Black Sea Journal of Engineering and Science, 9*(1), 254–264.

1. Introduction

Graphene nanoplatelets (GPLs) are high-strength materials with a thickness of several nanometers. Interest in graphene increased rapidly with the development of nanotechnology. Since they are produced entirely from graphite, they can conduct excellent thermal and electrical conduction. GPLs have been proven to be excellent candidates for enhancing material properties when added to the polymer matrix. For this reason, GPLs are widely used in the production of strong adhesives, in the reinforcement of structural elements, change of electrical properties, and in many other areas (Lee et al., 2008; Fei et al., 2020; Gaj et al., 2020; Kong et al., 2020; Songsuwan et al., 2021). The strength of graphene nanoplatelets is much higher than carbon nanotubes. By adding only %1 weight fraction of GPLs compared to %1 weight fraction of carbon nanotubes (CNTs), equivalent strength and stiffness can be obtained (Thai et al., 2020). Functionally graded material (FGM) is made by gradually combining two materials. The properties of the material can be described as smooth and continuous in spatial directions (Wattanasakulpong and Bui, 2017; Wattanasakulpong et al., 2018; Jalei and Civalek, 2019; Kim et al., 2019; Zur et al., 2020). By using such a concept, the structural performance of new composites can be improved significantly, especially for GPL-based composites. Therefore, the GPL-based composites produced in the form of FGMs are called functionally graded graphene nanoplatelet reinforced composites (FG-GPLRC) (Hao et al., 2019; Song et al., 2017; Gao et al., 2020). The studies correspond to the FG-GPLRC structures that examine the mechanical behaviors of composite structures that are in their infancy. The production of high-strength and slender beams, plates, and shells using this material and, the examination of the mechanical properties of these elements have recently attracted a lot of attention from engineers (Zhao et al., 2020). Yang et al. devoted great effort to the bending, buckling, and vibration behavior of FG-GPLRC beams and plates (Yang et al., 2017a; Yang et al., 2017b; Zhao et al., 2017; Song et al., 2018; Yang et al., 2018a). Lin et al. (2017) determined graphene efficiency parameters of FG-GPLRCs that were used to evaluate the material properties of the composite using these parameters by matching results from the Halpin–Tsai model and molecular dynamics simulations. Furthermore, Shen et al. discussed various results for nonlinear bending, vibration, and buckling behaviors of FG-GPLRC plates, panels, and shells (Shen et al., 2017a; Shen et al., 2017b; Shen et al., 2017c; Shen and Xiang, 2018; Shen et al., 2018). A large number of researchers have been carried out on building elements produced with reinforced materials with the help of GPLs. Some of these are; the vibration of pre-twisted panels reinforced by GPLs (Niu et al., 2019), linear and nonlinear analyses for buckling and vibration of FG-GPLRC piezoelectric plates under electric and mechanical forces (Mao and Zhang, 2018; Mao and Zhang, 2019), the vibration of FG-GPLRC doubly

curved shells (Wang et al., 2018; Wang et al., 2019a), FG-GPLRC structures with di-electric plates (Wang et al., 2019a). Moreover, the trend of investigations into FG-GPLRC structures has grown dramatically in the engineering community (Yang et al., 2018b; Thai et al., 2019; Karami and Shahsavari, 2020).

In addition to numerical and theoretical investigations, recent studies have increasingly focused on the experimental characterization of graphene nanoplatelet-reinforced structural elements. Saleh et al. (2025) conducted laboratory-scale experimental tests on reinforced concrete beams incorporating engineered nanographene and demonstrated significant improvements in flexural and shear performance, highlighting the strong influence of GPL content on structural behavior. Similarly, Yager et al. (2024) investigated the time-dependent mechanical properties of graphene nanoplatelet-reinforced concrete and reported notable enhancements in stiffness and long-term performance under sustained loading. On the numerical side, Ni et al. (2023) provided a detailed vibration analysis of graphene nanoplatelet-reinforced structures, offering valuable insights into damping and dynamic response characteristics. These recent experimental and numerical findings underline the practical relevance of GPL-reinforced composites and further motivate the development of reliable higher-order theoretical models for FG-GPLRC beams, particularly for capturing nonlinear bending behavior under different material gradation schemes.

In the modeling of functionally graded beam and plate structures, various classical and refined beam theories have been developed to capture shear deformation and thickness-dependent material behavior. Among these, higher-order shear deformation theories (HSDTs) have been shown to provide improved accuracy without the need for shear correction factors, particularly for moderately thick beams and structures with strong material gradation (Reddy, 1984). Subsequent developments extended these concepts to functionally graded micro- and macro-scale beams, demonstrating the effectiveness of higher-order kinematic assumptions in predicting bending and vibration responses (Simsek and Reddy, 2013). Comprehensive reviews further indicate that HSDT-based formulations constitute a robust theoretical framework for the analysis of functionally graded structures when compared to classical and first-order theories (Thai and Kim, 2015). Motivated by these established theoretical foundations, the present study adopts a higher-order beam formulation to investigate the nonlinear behavior of functionally graded graphene nanoplatelet-reinforced composite beams.

In the studies given above, it is assumed that the FG-GPLRC constructs have been produced as multi-layered GPLs. With this assumption, it is very difficult to account for stress concentrations and adhesion problems between layers. To circumvent these difficulties is to assume that the GPLs are continuously dispersed in the polymer matrix (Wang et al., 2019b; Wang et al., 2019c).

In this study, it was accepted that GPLs change softly along the beam height with the function proposed by Touratier. Total Potential energy is written taking into account nonlinear terms. The boundary conditions and equilibrium equations were found using the condition that the variation in energy is zero. The solution to the problem for various end conditions and loads is given numerically. The comprehensive literature review indicates that similar boundary conditions and equilibrium equations have not been previously formulated in the same manner.

2. Materials and Methods

2.1. FG-GPLRC Beams

The effective Young's modulus of composites made from GPLs/epoxy ($E_c(z)$) is composed of two modulus types: longitudinal ($E_l(z)$) and transverse ($E_t(z)$) modulus (Songsuwan et al., 2021; Wang et al., 2019c; Yang et al., 2017). In this study, a homogenized material model based on an effective modulus ($E_c(z)$) is adopted. The influence of graphene nanoplatelet orientation is therefore not explicitly considered and may affect local deformation characteristics under high bending moments. This limitation has been acknowledged, as the present formulation aims to capture the global nonlinear response of FG-GPLRC beams rather than detailed microscale effects (equations 1-5).

$$E_c(z) = \frac{3}{8}E_l(z) + \frac{5}{8}E_t(z) \tag{1}$$

$E_l(z)$ and $E_t(z)$ are

$$E_l = \frac{(1+\xi_l\eta_l V_{gpl})E_m}{1-\eta_l V_{gpl}} \tag{2}$$

$$E_t = \frac{(1+\xi_w\eta_w V_{gpl})E_m}{1-\eta_w V_{gpl}} \tag{3}$$

Where

$$\xi_l = \frac{2l_{gpl}}{h_{gpl}}, \xi_w = \frac{2w_{gpl}}{h_{gpl}}, \eta_l = (\frac{E_{gpl}}{E_m}-1)/(\frac{E_{gpl}}{E_m}+\xi_l)$$

$$\eta_w = (\frac{E_{gpl}}{E_m}-1)/(\frac{E_{gpl}}{E_m}+\xi_w) \tag{4}$$

$$V_{gpl} = \frac{g_{gpl}}{g_{gpl}+\frac{\rho_{gpl}(1-g_{gpl})}{\rho_m}}, g_{gpl} = \Psi_2(\frac{1}{2}-z),$$

$$V_m = 1 - V_{gpl} \tag{5}$$

where g_{gpl} is the given weight fraction, ρ_m and ρ_{gpl} denote the material density of the polymer matrix and GPLs, respectively

Poisson's ratio ($\nu_c(z)$) can be defined using the rule of mixtures as follows (equations 6 and 7):

$$\nu_c(z) = \nu_{gpl}V_{gpl} + \nu_m V_m \tag{6}$$

where

$$V_m = 1 - V_{gpl} \tag{7}$$

ν_{gpl} and ν_m are the Poisson's ratio of GPLs and polymer matrix, respectively. Numerical values of parameters and the form of weight fraction (g_{gpl}) are (Thai et al., 2019) (equation 8).

$\Psi_2 = 2, E_{gpl} = 1.01 TPa, v_{gpl}=0.186, \rho_{gpl}=1.06\ g/cm^3$
$E_m = 2.85\ GPa, v_m = 0.34, \rho_m = 1.2\ g/cm^3, l_{gpl}=2.5\ \mu m$
$w_{gpl} = 1.5\ \mu m, h_{gpl} = 1.5\ \mu m, g_{gpl} = \Psi_2\ (\frac{1}{2} - z)$ (8)

3. Results

The graph of the Youngs modulus for the values of the parameters given in equation 8 is shown in Figure 1.

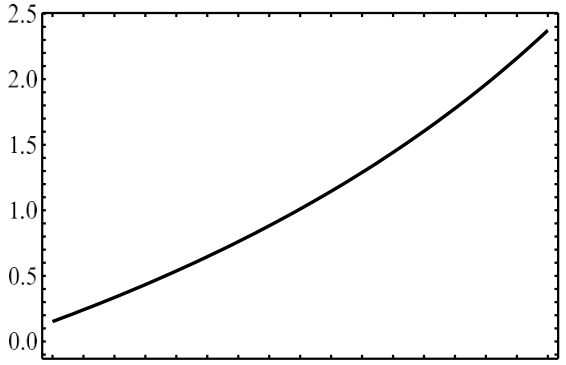

Figure 1. Variation of Young's modulus $E_c(z)$ (vertical axis) along the beam thickness (z/h, horizontal axis).

3.1. Beam Under Consideration

Figure 2 presents geometry of the FG-GPLRC beam and its cross-section.

Figure 2. Geometry of the FG-GPLRC beam and its cross-section.

The displacement field of the shear deformation theory is expressed as follows (Wang et al., 2019c; Simsek and Reddy, 2013; Joshan et al., 2017; Singh and Singh, 2017).

$$u(x,z) = u_0(x) - zw'(x) + f(z)\varphi(x) \quad (9)$$

$$w(x,z) = w(x) \quad (10)$$

where prime means the derivative of $w(x)$ with respect to x, u and w de- note the displacement components of the beam at any point, u_0 is the axial displacement at any point on the mid-plane surface (z = 0) of the beam, φ represents the shear deformation at the mid-plane surface, and f (z) represents the shear-strain function that corresponds only to the function of thickness coordinate z. Normal strain ϵ_{xx} and shear strain γ_{xz} relations are found by taking into account the nonlinear terms with the help of 9 and 10 relations as follows (equations 11-16).

$$\epsilon_{xx} = \frac{\partial u}{\partial x} + \frac{1}{2}(\frac{\partial w}{\partial x})^2 \quad (11)$$

$$\gamma_{xx} = \frac{\partial u}{\partial x} + \frac{\partial w}{\partial x} \quad (12)$$

$$\epsilon_{xx} = u_0{}' - zw'' + f\varphi' + \frac{1}{2}w'^2 \quad (13)$$

$$\gamma_{xx} = f\varphi' \quad (14)$$

$$\sigma_x = E_c(z)\epsilon_{xx} = E_c u_0' - E_c z w'' + E_c f\varphi' + \frac{1}{2}E_c w'^2 \quad (15)$$

$$\tau_{xz} = G_C(z)\gamma_{xz} = G_C f'\varphi \quad (16)$$

where Gc(z) is shear modulus. Variation of total energy is

$$\delta\pi = \int_0^L \int_{-\frac{b}{2}}^{\frac{b}{2}} \int_{-\frac{h}{2}}^{\frac{h}{2}} (\sigma_x \delta\epsilon_{xx} + \tau_{xz}\delta\gamma_{xx}) dy dz dx - \int_0^L q(x)\delta w dx \quad (17)$$

If equations 11, 12, 13, 14, 15 and 16 are used, the following relation is obtained (equations 18 and 19).

$$\delta\pi = c_6 \int_0^L u_0{}' \delta u_0' dx - c_3 \int_0^L u_0{}' \delta w'' dx + c_5 \int_0^L u_0{}' \delta\varphi' dx + c_6 \int_0^L u_0{}' w' \delta w' dx - c_3 \int_0^L w'' \delta u_0' dx + c_1 \int_0^L w'' \delta w'' dx - c_2 \int_0^L w'' \delta\varphi' dx - c_3 \int_0^L w'' w' \delta w' dx + c_5 \int_0^L \varphi' \delta u_0' dx - c_2 \int_0^L \varphi' \delta w'' dx + c_4 \int_0^L \varphi' \delta\varphi' dx + c_5 \int_0^L \varphi' w' \delta w' dx + \frac{c_6}{2} \int_0^L w'^3 \delta u_0' dx - \frac{c_3}{2} \int_0^L w'^2 \delta w'' dx + \frac{c_5}{2} \int_0^L w'^2 \delta\varphi' dx + \frac{c_6}{2} \int_0^L w'^3 \delta w' dx + c_7 \int_0^L \varphi\, \delta\varphi dx - \int_0^L q\, \delta w dx \quad (18)$$

Where

$$c_1 = b \int_{-\frac{h}{2}}^{\frac{h}{2}} z^2 E_c(z) dz, \quad c_2 = b \int_{-\frac{h}{2}}^{\frac{h}{2}} z\, E_c(z) f(z) dz, \quad c_3 = b \int_{-\frac{h}{2}}^{\frac{h}{2}} z\, E_c(z) dz, \quad c_4 = b \int_{-\frac{h}{2}}^{\frac{h}{2}} E_c(z) f(z)^2 dz, c_5 = b \int_{-\frac{h}{2}}^{\frac{h}{2}} E_c(z) f(z) dz, \quad c_6 = b \int_{-\frac{h}{2}}^{\frac{h}{2}} E_c(z) dz, \quad c_7 = b \int_{-\frac{h}{2}}^{\frac{h}{2}} G_c(z) f'(z)^2 dz, \quad (19)$$

Function $f(z)$ for shear stress distribution is selected as Touratier's model (Touratier, 1991; Wang et al., 2019c) (equation 20).

$$f(z) = \frac{h}{\pi} \sin\frac{\pi z}{h} \quad (20)$$

With the help of the minimum total potential energy principle ($\delta\pi = 0$), the boundary conditions and governing equations are obtained as follows. Boundary conditions are (equations 21-28);

$$N\delta u_0|_0^L = 0 \quad (21)$$

$$T\delta w|_0^L = 0 \quad (22)$$

$$M_1\delta w'|_0^L = 0 \quad (23)$$

$$M_2\delta\varphi|_0^L = 0 \quad (24)$$

Where

$$N = c_6 u_0' - c_3 w'' + c_5\varphi' + \frac{c_6}{2} w'^2 \quad (25)$$

$$T = c_3 u_0'' - c_6 u_0' w' - c_1 w''' + c_2\varphi'' + c_5\varphi' w' + \frac{c_6}{2} w'^3 \quad (26)$$

$$M_1 = -c_3 u_0{}' + c_1 w'' - c_2 \varphi' - \frac{c_3}{2} w'^2 \quad (27)$$

$$M_2 = c_5 u_0{}' - c_2 w'' + c_4 \varphi' + \frac{c_5}{2} w'^2 \quad (28)$$

Equlibrium equations are (equations 29-31).

$$N'(x) = 0 \quad (29)$$

$$T'(x) = -q(x) \quad (30)$$

$$M_2'(x) - c_7 \varphi(x) = 0 \quad (31)$$

The dimensionless quantities are defined as follows (equation 32).

$$\bar{T} = \frac{T}{c_6},\ \bar{N} = \frac{N}{c_6},\ \overline{M_1} = \frac{M_1}{c_6 L},\ \overline{M_2} = \frac{M_2}{c_6 L},\ \alpha = \frac{b}{h},\ \overline{u_0} = \frac{u_0}{L},\ \overline{w_0} = \frac{w_0}{L},\ \bar{x} = \frac{x}{L},\ \bar{q}(x) = q(x)\frac{L}{c_6} \quad (32)$$

Equilibrium equations take the following form in terms of dimensionless quantities (equations 33-35).

$$\frac{c_6 L\left(\bar{u}''(\bar{x}) + \bar{w}'(\bar{x})\bar{w}''(\bar{x})\right) - c_3 \bar{w}^{(3)}(\bar{x}) + c_5 \varphi''(\bar{x})}{c_6 L} = 0 \quad (33)$$

$$\frac{c_3 L \bar{u}^{(3)}(\bar{x}) + c_5 L\left(\bar{w}''(\bar{x})\varphi'(\bar{x}) + \bar{w}'(\bar{x})\varphi''(\bar{x})\right) - c_1 \bar{w}^{(4)}(\bar{x}) + c_2 \varphi^{(3)}(\bar{x})}{c_6 L} + \bar{q}(\bar{x}) + u''(\bar{x})\bar{w}'^{(\bar{x})} + \bar{u}'(\bar{x})\bar{w}''(\bar{x}) + \frac{3}{2}\bar{w}'(\bar{x})^2 \bar{w}''(\bar{x}) = 0 \quad (34)$$

$$\frac{-c_7 L^2 \varphi(\bar{x}) + c_5 L\left(u''(\bar{x}) + w'(\bar{x})w''(\bar{x})\right) - c_2 w^{(3)}(\bar{x}) + c_4 \varphi''(\bar{x})}{c_6 L} = 0 \quad (35)$$

3.2. Examples

Simple beams and two-end fixed beams under the influence of different types of loads are examined in the examples below.

3.2.1. The simple beam is subjected to a uniform load

Figure 3 presents a simple beam is subjected to a uniform load.

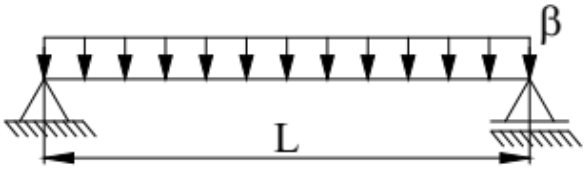

Figure 3. A simple beam is subjected to a uniform load.

In this example, the axial displacement $\bar{u}_0$ in $\bar{x} = 1$ is not zero. With the help of the boundary condition given by the relation of 21, the axial force is obtained as $\bar{N} = 0$. The boundary conditions are (equations 36-44).

$$\bar{M}_1(0) = 0, \bar{M}_2(0) = 0, \bar{w}(0) = 0, \bar{T}_2(0) = \frac{\bar{\beta}}{2}$$

$$\bar{M}_1(1) = 0, \bar{M}_2(1) = 0, \bar{w}(1) = 0, \bar{T}_2(1) = -\frac{\bar{\beta}}{2} \quad (36)$$

Vertical displacements ($\bar{w}$), axial displacements ($\bar{u}_0$), rotation of cross-sections φ, moments $\bar{M}_1$, $\bar{M}_2$ and shear force $\bar{T}$ are obtained by numerically with the help of governing equations (29, 30, 31) and boundary conditions for a simple beam subjected to a uniform load (Figures 3, 4, 5,6, 7, 8, 9 and equations 37, 38, 39, 40, 41 42, 43, 44). Selected parameters are given below.

$$\alpha = \frac{1}{2}, L = 1m, h = 0.8m, b = \alpha h, \beta = 1N/m \quad (37)$$

Numerical values of c_i coefficients are

$c_1 = 0.0197809, c_2 = 0.0152049,\ c_3 = 0.0463755,\ c_4 = 0.011857,\ c_5 = 0.0358353,\ c_6 = 0.349531,\ c_7 = 0.0694033$ (38)

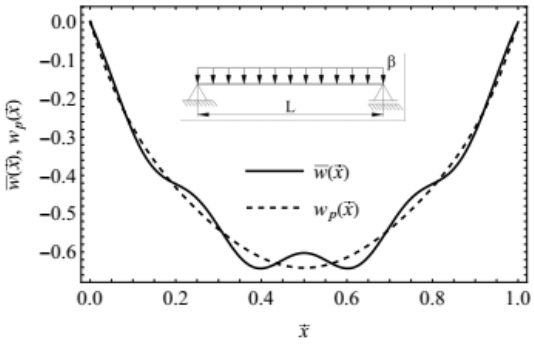

Figure 4. Vertical displacements.

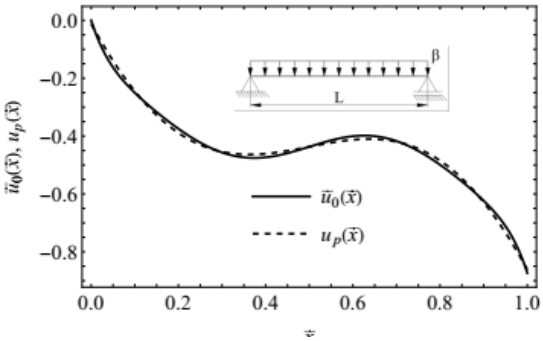

Figure 5. Axial displacements.

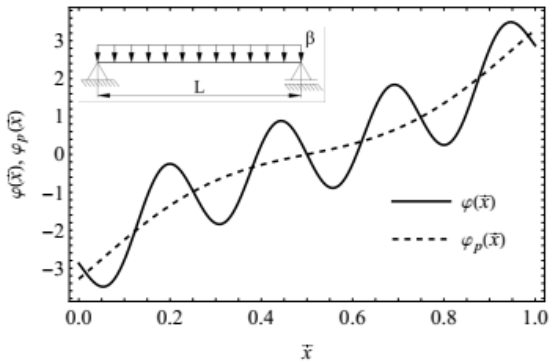

Figure 6. Rotation of cross-sections.

$$w_p(x) = 24.598x^6 - 73.7952x^5 + 85.4561x^4 - 47.9202x^3 + 15.624x^2 - 3.96309x + 0.00508682 \quad (39)$$

$$u_p(x) = 2.86476x^5 - 7.1619x^4 + 1.87407x^3 + 4.35079x^2 - 2.77764x - 0.0119582 \quad (40)$$

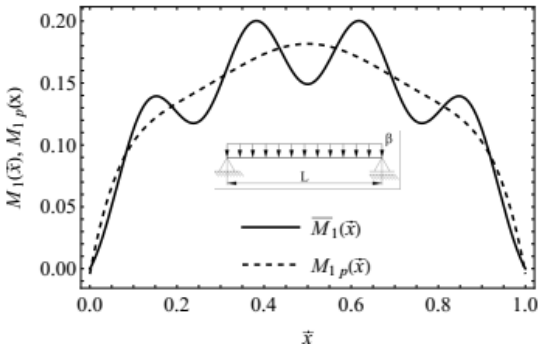

Figure 7. Moment-M_1.

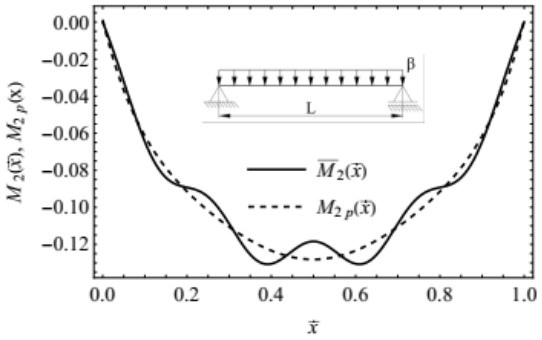

Figure 8. Moment-M_2.

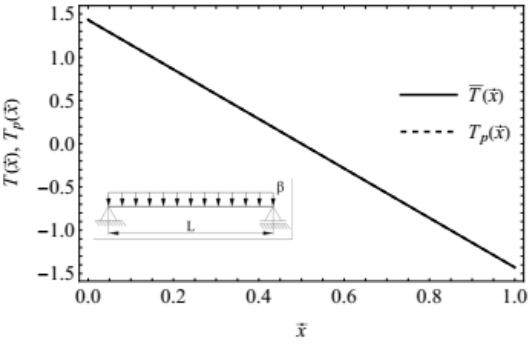

Figure 9. Shear force.

$$\varphi_p(x) = -0.0000543558x^6 - 36.4423x^5 + 91.106x^4 - 65.6862x^3 + 7.42331x^2 + 10.1733x - 3.287 \quad (41)$$

$$M_{1p}(x) = 20.6875x^6 + 62.0625x^5 - 71.8694x^4 + 40.3013x^3 - 11.7094x^2 + 1.90251x - 0.00427806 \quad (42)$$

$$M_{2p}(x) = 6.28831x^6 - 18.8649x^5 + 22.1359x^4 - 12.8302x^3 + 4.21323x^2 - 0.942298x + 0.00127271 \quad (43)$$

$$T_p(x) = 1.43049 - 2.86098x - 0.0000293798x^2 + 0.000208642x^3 - 0.000516923x^4 + 0.00054273x^5 - 0.000204722x^6 \quad (44)$$

3.2.2. The simple beam is subjected to a triangular load

Figure 10 presents simple beam is subjected to a triangular load.

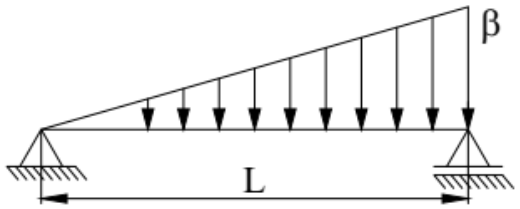

Figure 10. Simple beam is subjected to a triangular load

In this example, the axial displacement ($\bar{u}_0$) in $\bar{x} = 1$ is not zero. With the help of the boundary condition given by the relation of 21, the axial force is obtained as $\bar{N} = 0$. The boundary conditions are (equation 45).

$$\bar{M}_1(0) = 0, \bar{M}_2(0) = 0, \bar{w}(0) = 0, \bar{T}_2(0) = \frac{\bar{\beta}}{2}$$
$$\bar{M}_1(1) = 0, \bar{M}_2(1) = 0, \bar{w}(1) = 0, \bar{T}_2(1) = -\frac{\bar{\beta}}{2} \quad (45)$$

Vertical displacements $\bar{w}$, axial displacements $\bar{u}_0$, rotation of cross-sections φ, moments $\bar{M}_1$, $\bar{M}_2$ and shear force $\bar{T}$ are obtained by numerically with the help of equilibrium equations (29, 30, 31) and boundary conditions for a simple beam subjected to a uniform load (Figures 10, 11, 12,13, 14, 15,16 and equations 46, 47, 48 49, 50, 51). Selected parameters and ci coefficients are given in equations 37 and 38

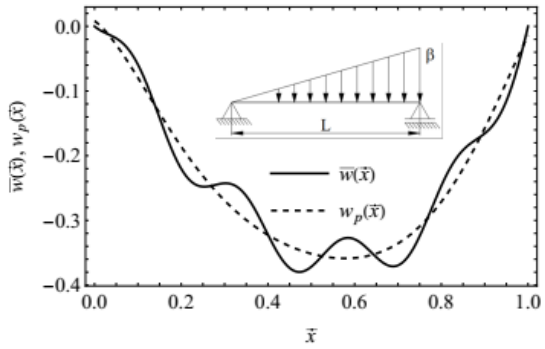

Figure 11. Vertical displacements.

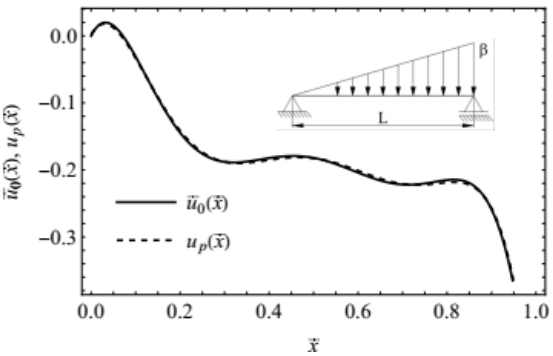

Figure 12. Axial displacements.

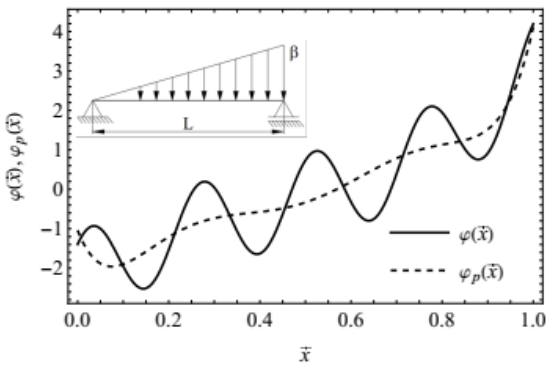

Figure 13. Rotation of cross-sections.

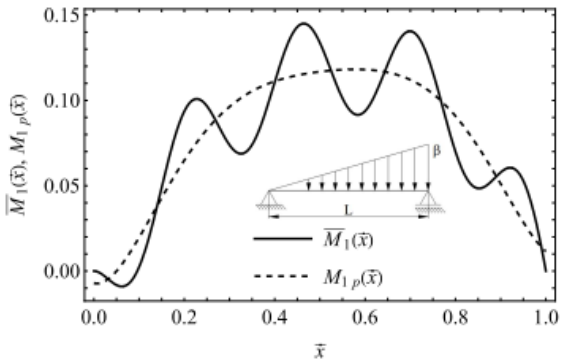

Figure 14. Moment-M_1.

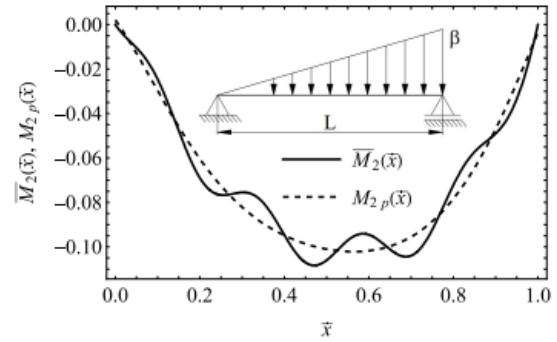

Figure 15. Moment-M_2.

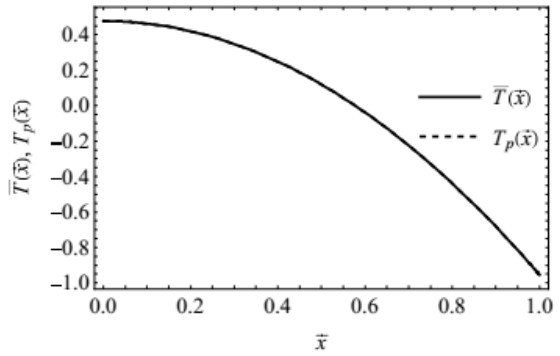

Figure 16. Shear force.

$$w_p(x) = -12.3586x^6 + 38.3878x^5 - 45.2305x^4 + 25.6918x^3 - 6.02133x^2 - 0.49134x + 0.00841133 \quad (46)$$

$$u_p(x) = -70.568x^6 + 201.252x^5 - 217.898x^4 + 109.525x^3 - 24.1045x^2 + 1.16614x + 0.00190374 \quad (47)$$

$$\varphi_p(x) = 670.431x^6 - 1983.15x^5 + 2242.22x^4 - 1204.36x^3 + 309.582x^2 - 29.5714x - 1.03818 \quad (48)$$

$$M_{1p}(x) = 10.3937x^6 - 32.2845x^5 + 38.0393x^4 - 21.1303x^3 + 5.064x^2 - 0.0636072x - 0.00707401 \quad (49)$$

$$M_{2p}(x) = -2.97564x^6 + 9.32188x^5 - 10.8194x^4 + 5.79088x^3 - 1.06437x^2 - 0.258937x + 0.00210673 \quad (50)$$

$$T_p(x) = -0.000116502x^6 + 0.00032794x^5 - 0.000333841x^4 + 0.000146841x^3 - 1.43051x^2 + 1.100207 * 10^{-6}x + 0.476829 \quad (51)$$

3.2.3. Two-end fixed beam under uniformly distributed load

Figure 17 presents two-end fixed beam under uniformly distributed load.

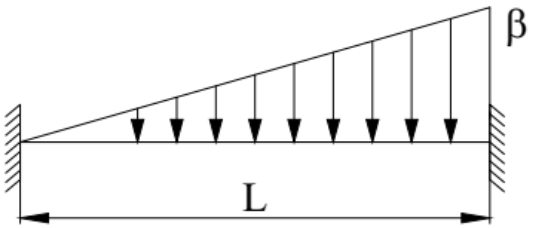

Figure 17. Two-end fixed beam under uniformly distributed load.

The boundary conditions are (equation 52).

$$\bar{w}(0) = 0, \quad \bar{w}'(0) = 0, \quad \bar{\varphi}(0) = 0$$
$$\bar{w}(1) = 0, \quad \bar{w}'(1) = 0, \quad \bar{\varphi}(1) = 0 \quad (52)$$

Selected parameters and c_i coefficients are (equations 53 and 54)

$$\alpha = \frac{1}{4}, L = 0.06m, h = 0.6m, b = \alpha h, \beta = 10N/m \quad (53)$$

$$c_1 = 0.00294949, c_2 = 0.0022738, c_3 = 0.0072335, c_4 = 0.00177848, \; c_5 = 0.00559372, \quad c_6 = 0.0950059, c_7 = 0.0193613 \quad (54)$$

Axial force $\bar{N}$, Vertical displacements $\bar{w}$, axial displacements $\bar{u}_0$, rotation of cross-sections φ, moments $\bar{M}_1$, $\bar{M}_2$ and shear force $\bar{T}$ are obtained by numerically with the help of equilibrium equations (29, 30, 31) and boundary conditions for a fixed-end beam subjected to a uniform load (Figure 17). Dimensionless axial force is found as $\bar{N}$= 4.6. (Figures 18, 19,20, 21, 22, 23 and equations 46-60).

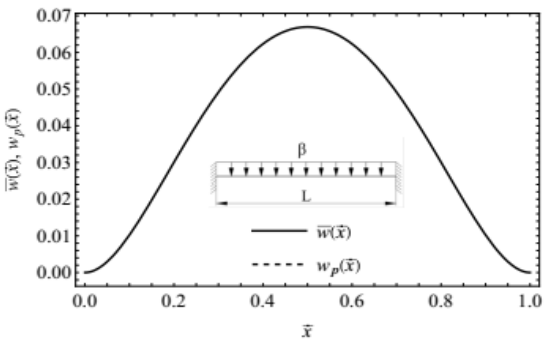

Figure 18. Vertical displacements.

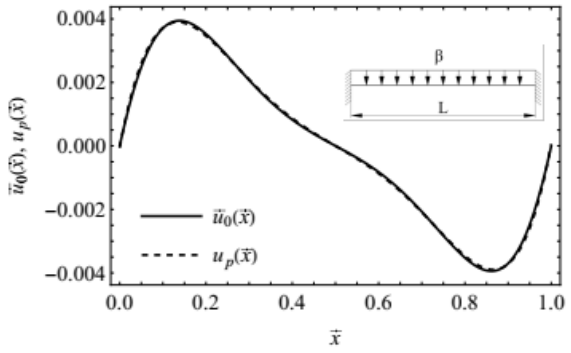

Figure 19. Axial displacements.

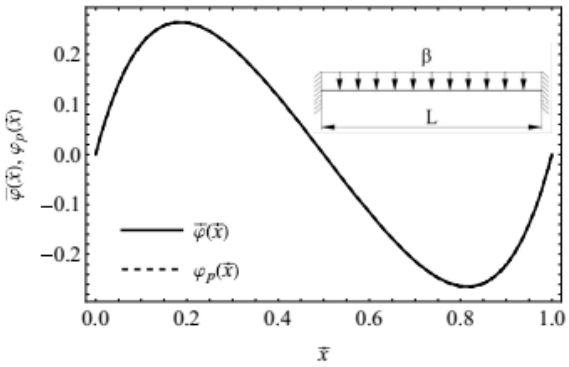

Figure 20. Rotation of cross-sections.

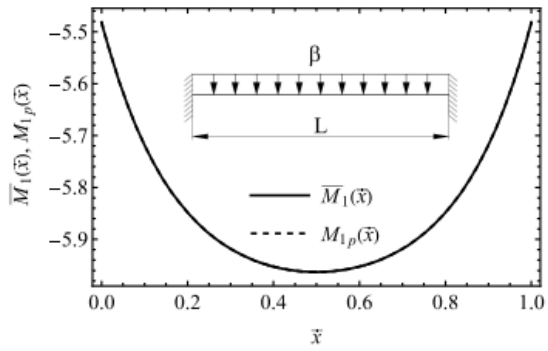

Figure 21. Moment-M_1.

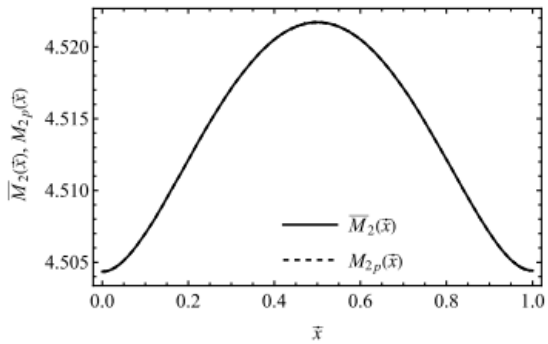

Figure 22. Moment-M_2.

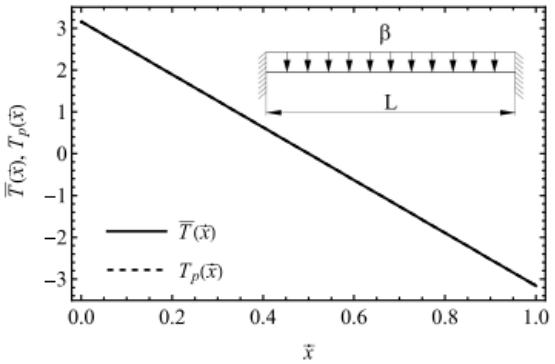

Figure 23. Shear force.

$$w_p(x) = 1.07242x^6 - 3.21725x^5 + 4.54465x^4 - 3.72722x^3 + 1.32449x^2 + 0.00291524x - 0.0000109887 \quad (55)$$

$$u_p(x) = -0.0000164922x^6 + 0.452401x^5 - 1.13095x^4 + 1.05x^3 - 0.444066x^2 + 0.0727426x - 0.0000562965 \quad (56)$$

$$\varphi_p(x) = 0.0000232329x^6 + 8.67725x^5 - 21.6932x^4 + 24.2411x^3 - 14.6684x^2 + 3.4419x + 0.000673838 \quad (57)$$

$$M_{1p}(x) = 4.93259x^6 - 14.7982x^5 + 20.9045x^4 - 17.1449x^3 + 9.25028x^2 - 3.14429x - 5.48145 \quad (58)$$

$$M_{2p}(x) = 0.279462x^6 - 0.837942x^5 + 1.18252x^4 - 0.968706x^3 + 0.343992x^2 + 0.00075917x + 4.50433 \quad (59)$$

$$T_p(x) = 0.00357093x^6 - 0.0071751x^5 + 0.00628797x^4 - 0.00252181x^3 + 0.000553832x^2 - 6.31545x + 3.1577 \quad (60)$$

3.2.4. Two-end fixed beam is subjected to a triangular load

Figure 24 presents two-end fixed beam is subjected to a triangular load.

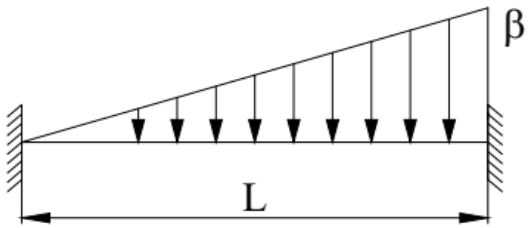

Figure 24. Two-end fixed beam is subjected to a triangular load

The boundary conditions are (equations 61).

$$\bar{w}(0) = 0, \quad \bar{w}'(0) = 0, \quad \bar{\varphi}(0) = 0$$
$$\bar{w}(1) = 0, \quad \bar{w}'(1) = 0, \quad \bar{\varphi}(1) = 0 \quad (61)$$

Selected parameters and c_i coefficients are given in equations 53 and 54

Axial force $\bar{N}$, Vertical displacements $(\bar{w})$, axial displacements $(\bar{u}_0)$, rotation of cross-sections φ, moments $\bar{M}_1$, $\bar{M}_2$ and shear force $\bar{T}$ are obtained by numerically with the help of equilibrium equations (29, 30, 31) and boundary conditions for a fixed-end beam subjected to a triangular load (Figure 24).

Dimensionless axial force is found as $\bar{N} = 5$. (Figures 25, 26, 27, 28, 29, 30 and equations 62-67)ç

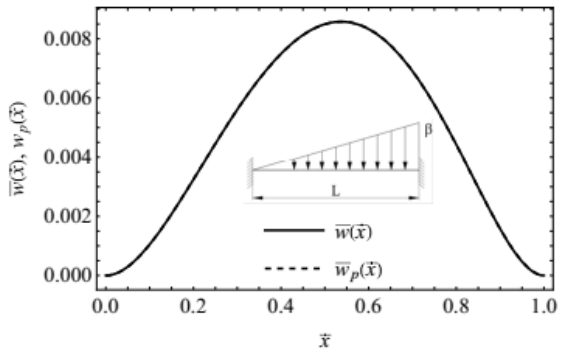

Figure 25. Vertical displacements.

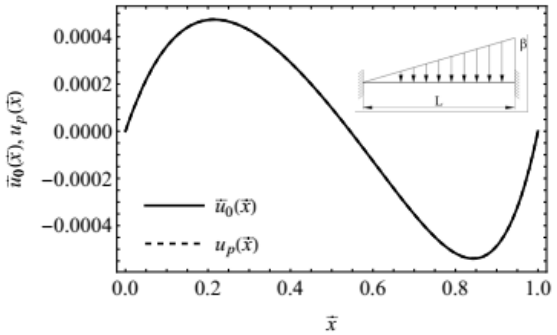

Figure 26. Axial displacements.

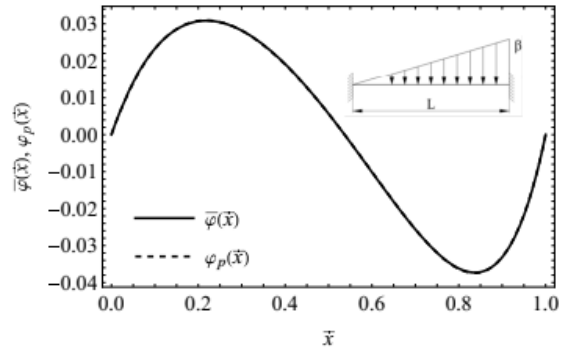

Figure 27. Rotation of cross-sections.

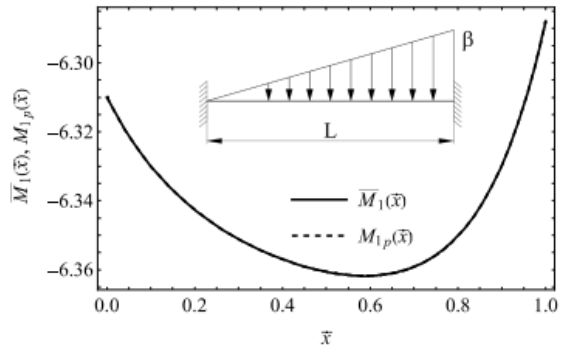

Figure 28. Moment-M_1.

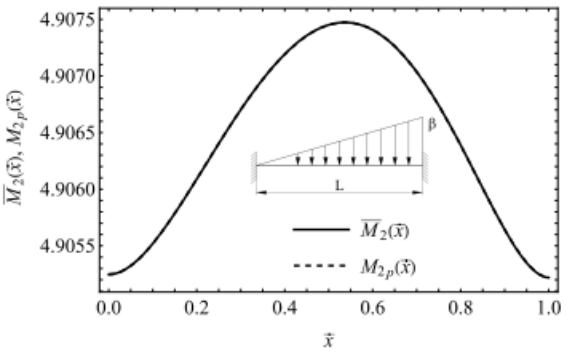

Figure 29. Moment-M_2.

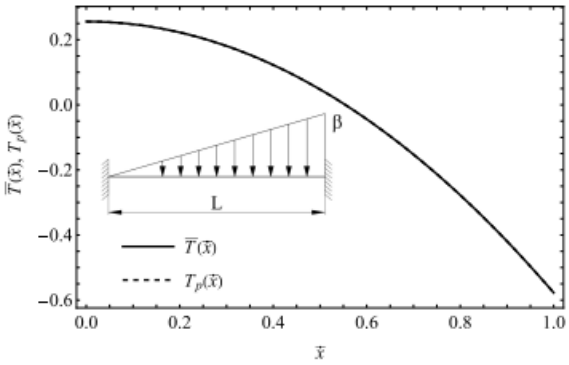

Figure 30. Shear force.

$$w_p(x) = 0.144126x^6 - 0.365661x^5 + 0.435825x^4 - 0.352751x^3 + 0.138827x^2 - 0.000377659x + 3.975704 * 10^{-6} \quad (62)$$

$$u_p(x) = 0.0132266x^6 - 0.0193753x^5 + 0.000283115x^4 + 0.0182054x^3 - 0.0174929x^2 + 0.00515248x + 5.411311 * 10^{-7} \quad (63)$$

$$\varphi_p(x) = 0.576675x^6 - 0.559113x^5 - 0.516918x^4 + 1.28968x^3 - 1.12158x^2 + 0.331066x + 0.000091323 \quad (64)$$

$$M_{1p}(x) = 0.720841x^6 - 1.82873x^5 + 2.17949x^4 - 1.48611x^3 + 0.694158x^2 - 0.257732x - 6.30986 \quad (65)$$

$$M_{2p}(x) = 0.0373309x^6 - 0.0948297x^5 + 0.113099x^4 - 0.0915632x^3 + 0.0360297x^2 - 0,0000976065x + 4.90525 \quad (66)$$

$$T_p(x) = -0.00139672x^6 + 0.00285179x^5 - 0.00249386x^4 + 0.00100571x^3 - 0.833547x^2 + 0.0000186903x + 0.255842 \quad (67)$$

4. Discussion

In this study, the nonlinear bending behavior of functionally graded graphene nanoplatelet reinforced composite (FG-GPLRC) beams has been investigated by high-order shear deformation theory (HSDT). The governing equilibrium equations and boundary conditions were derived based on the minimum total potential energy principle. The formulation incorporates two distinct bending moment components associated with axial rotation and cross-sectional rotation, enabling a more refined

representation of beam kinematics.

The derived equilibrium equations are general in nature and can be adapted to different beam theories by modifying the shear strain function f(z). In this context, Touratier's higher-order model was employed to demonstrate the applicability of the formulation. The results indicate that the proposed framework can be effectively extended to analyze not only nonlinear bending but also vibration and buckling behavior of FG-GPLRC beams.

Numerical solutions were obtained for various boundary conditions and loading cases, and the spatial variation of key response quantities along the beam length was presented graphically. Polynomial expressions fitted to the numerical results were also provided, offering a practical means for verification and further analytical use.

It can be concluded that the proposed formulation provides a versatile and consistent theoretical framework for the analysis of FG-GPLRC beams. The results establish a foundation for future comparative studies with experimental data, which may further clarify the applicability of higher-order beam models, such as Touratier's theory, to different classes of functionally graded composite beams.

Author Contributions

The percentages of the authors' contributions are presented below. All authors reviewed and approved the final version of the manuscript.

	R.A.	İ.Ö.K.
C	50	50
D	50	50
S	50	50
L	50	50
W	50	50
CR	50	50
SR	50	50
PM	50	50
FA	50	50

C=Concept, D= design, S= supervision, L= literature search, W= writing, CR= critical review, SR= submission and revision, PM= project management, , FA= funding acquisition.

Conflict of Interest

The author declared that there is no conflict of interest.

Ethical Consideration

Ethics committee approval was not required for this study because of there was no study on animals or humans.

Acknowledgements

The work reported here is supported by the Alexander von Humboldt Foundation.

References

Fei, Y., Fang, S., & Hu, Y. H. (2020). Synthesis, properties and potential applications of hydrogenated graphene. *Chemical Engineering Journal, 397*, 125408. https://doi.org/10.1016/j.cej.2020.125408

Gaj, J., Clapa, M., Nowak, D., Juszczak, J., Galazka, M., Pelka, M., & Niedzielski, P. (2020). Metallurgical graphene under different gas atmospheres and UV radiation for gas-sensing applications. *Sensors and Actuators A: Physical, 312*, 112152. https://doi.org/10.1016/j.sna.2020.112152

Gao, K., Do, D. M., Li, R., Kitipornchai, S., & Yang, J. (2020). Probabilistic stability analysis of functionally graded graphene reinforced porous beams. *Aerospace Science and Technology, 98*, 105738. https://doi.org/10.1016/j.ast.2020.105738

Hao, Y. X., Cao, Z., Zhang, W., Chen, J., & Yao, M. H. (2019). Stability analysis for geometric nonlinear functionally graded sandwich shallow shell using a new developed displacement field. *Composite Structures, 210*, 202–216. https://doi.org/10.1016/j.compstruct.2018.11.053

Jalei, M. H., & Civalek, O. (2019). On dynamic instability of magnetically embedded viscoelastic porous FG nanobeam. *International Journal of Engineering Science, 143*, 14–32. https://doi.org/10.1016/j.ijengsci.2019.06.012

Joshan, Y. S., Grover, N., & Singh, B. N. (2017). A new non-polynomial four variable shear deformation theory in axiomatic formulation for hygro-thermo-mechanical analysis of laminated composite plates. *Composite Structures, 182*, 685–693. https://doi.org/10.1016/j.compstruct.2017.09.052

Karami, B., & Shahsavari, D. (2020). On the forced resonant vibration analysis of functionally graded polymer composite doubly-curved nanoshells reinforced with graphene-nanoplatelets. *Computer Methods in Applied Mechanics and Engineering, 359*, 112767. https://doi.org/10.1016/j.cma.2019.112767

Kim, J., Zur, K. K., & Reddy, J. N. (2019). Bending, free vibration, and buckling of modified couple stress-based functionally graded porous micro-plates. *Composite Structures, 209*, 879–888. https://doi.org/10.1016/j.compstruct.2018.11.023

Kong, X., Zhu, Y., Lei, H., Wang, C., Zhao, Y., Huo, E., Lin, X., Zhang, Q., Qian, M., Mateo, W., Zou, R., Fang, Z., & Ruan, R. (2020). Synthesis of graphene-like carbon from biomass pyrolysis and its applications. *Chemical Engineering Journal, 399*, 125808. https://doi.org/10.1016/j.cej.2020.125808

Lee, C., Wei, X., Kysar, J. W., & Hone, J. (2008). Measurement of the elastic properties and intrinsic strength of monolayer graphene. *Science, 321*(5887), 385–388. https://doi.org/10.1126/science.1157996

Lin, F., Xiang, Y., & Shen, H. S. (2017). Temperature dependent mechanical properties of graphene reinforced polymer nanocomposites – A molecular dynamics simulation. *Composites Part B: Engineering, 111*, 261–269. https://doi.org/10.1016/j.compositesb.2016.12.004

Mao, J. J., & Zhang, W. (2018). Linear and nonlinear free and forced vibrations of graphene reinforced piezoelectric composite plate under external voltage excitation. *Composite Structures, 203*, 551–565. https://doi.org/10.1016/j.compstruct.2018.06.076

Mao, J. J., & Zhang, W. (2019). Buckling and post-buckling analyses of functionally graded graphene reinforced piezoelectric plate subjected to electric potential and axial forces. *Composite Structures, 216*, 392–405.

https://doi.org/10.1016/j.compstruct.2019.02.091

Ni, Z., Fan, Y., Hang, Z., Zhu, F., Wang, Y., Feng, C., & Yang, J. (2023). Damped vibration analysis of graphene nanoplatelet reinforced dielectric membrane using Taylor series expansion and differential quadrature methods. *Thin-Walled Structures, 184*, 110492. https://doi.org/10.1016/j.tws.2022.110492

Niu, Y., Zhang, W., & Guo, X. Y. (2019). Free vibration of rotating pretwisted functionally graded composite cylindrical panel reinforced with graphene platelets. *European Journal of Mechanics - A/Solids, 77*, 103798. https://doi.org/10.1016/j.euromechsol.2019.05.003

Reddy, J. N. (1984). A simple higher-order theory for laminated composite plates. *Journal of Applied Mechanics, 51*(4), 745–752. https://doi.org/10.1115/1.3167719

Saleh, A., Salem, H., & Fadallah, R. (2025). Experimental investigation of the effect of engineered nanographene on the flexure and shear behavior of reinforced concrete beams. *Journal of Engineering and Applied Science, 72*(1), 172. https://doi.org/10.1186/s44147-024-00628-9

Shen, H. S., Lin, F., & Xiang, Y. (2017a). Nonlinear bending and thermal postbuckling of functionally graded graphene-reinforced composite laminated beams resting on elastic foundations. *Engineering Structures, 140*, 89–97. https://doi.org/10.1016/j.engstruct.2017.02.069

Shen, H. S., Lin, F., & Xiang, Y. (2017b). Nonlinear vibration of functionally graded graphene-reinforced composite laminated beams resting on elastic foundations in thermal environments. *Nonlinear Dynamics, 90*(2), 899–914. https://doi.org/10.1007/s11071-017-3701-0

Shen, H. S., & Xiang, Y. (2018). Postbuckling behavior of functionally graded graphene-reinforced composite laminated cylindrical shells under axial compression in thermal environments. *Computer Methods in Applied Mechanics and Engineering, 330*, 64–82. https://doi.org/10.1016/j.cma.2017.10.023

Shen, H. S., Xiang, Y., Fan, Y., & Hui, D. (2018). Nonlinear vibration of functionally graded graphene-reinforced composite laminated cylindrical panels resting on elastic foundations in thermal environments. *Composites Part B: Engineering, 136*, 177–186. https://doi.org/10.1016/j.compositesb.2017.10.033

Shen, H. S., Xiang, Y., Lin, F., & Hui, D. (2017c). Buckling and post-buckling of functionally graded graphene-reinforced composite laminated plates in thermal environments. *Composites Part B: Engineering, 119*, 67–78. https://doi.org/10.1016/j.compositesb.2017.03.020

Simsek, M., & Reddy, J. N. (2013). Bending and vibration of functionally graded microbeams using a new higher order beam theory and the modified couple stress theory. *International Journal of Engineering Science, 64*, 37–53. https://doi.org/10.1016/j.ijengsci.2012.12.002

Singh, D. B., & Singh, B. N. (2017). New higher order shear deformation theories for free vibration and buckling analysis of laminated and braided composite plates. *International Journal of Mechanical Sciences, 131-132*, 265–277. https://doi.org/10.1016/j.ijmecsci.2017.07.013

Song, M., Kitipornchai, S., & Yang, J. (2017). Free and forced vibrations of functionally graded polymer composite plates reinforced with graphene nanoplatelets. *Composite Structures, 159*, 579–588. https://doi.org/10.1016/j.compstruct.2016.09.070

Song, M., Yang, J., & Kitipornchai, S. (2018). Bending and buckling analyses of functionally graded polymer composite plates reinforced with graphene nanoplatelets. *Composites Part B: Engineering, 134*, 106–113. https://doi.org/10.1016/j.compositesb.2017.09.043

Songsuwan, W., Prabkeao, C., & Wattanasakulpong, N. (2021). On linear and nonlinear bending of functionally graded graphene nanoplatelet reinforced composite beams using Gram-Schmidt Ritz method. *Mechanics Based Design of Structures and Machines, 51*(10), 5437–5463. https://doi.org/10.1080/15397734.2021.1983584

Thai, C. H., Ferreira, A. J. M., Tran, T. D., & Phung-Van, P. (2019). Free vibration, buckling and bending analyses of multilayer functionally graded graphene nanoplatelets reinforced composite plates using the NURBS formulation. *Composite Structures, 220*, 749–759. https://doi.org/10.1016/j.compstruct.2019.04.053

Thai, C. H., Ferreira, A. J. M., Tran, T. D., & Phung-Van, P. (2020). A size-dependent quasi-3D isogeometric model for functionally graded graphene platelet-reinforced composite microplates based on the modified couple stress theory. *Composite Structures, 234*, 111695. https://doi.org/10.1016/j.compstruct.2019.111695

Thai, H. T., & Kim, S. E. (2015). A review of theories for the modeling and analysis of functionally graded plates and shells. *Composite Structures, 128*, 70–86. https://doi.org/10.1016/j.compstruct.2015.03.035

Touratier, M. (1991). An efficient standard plate theory. *International Journal of Engineering Science, 29*(8), 901–916. https://doi.org/10.1016/0020-7225(91)90165-Y

Wang, A., Chen, H., Hao, Y., & Zhang, W. (2018). Vibration and bending behavior of functionally graded nanocomposite doubly-curved shallow shells reinforced by graphene nanoplatelets. *Results in Physics, 9*, 550–559. https://doi.org/10.1016/j.rinp.2018.02.063

Wang, Y., Feng, C., Wang, X., Zhao, Z., Romero, C. S., Dong, Y., & Yang, J. (2019a). Nonlinear static and dynamic responses of graphene platelets reinforced composite beam with dielectric permittivity. *Applied Mathematical Modelling, 71*, 298–315. https://doi.org/10.1016/j.apm.2019.02.023

Wang, Y., Xie, K., Fu, T., & Shi, C. (2019b). Bending and elastic vibration of a novel functionally graded polymer nanocomposite beam reinforced by graphene nanoplatelets. *Nanomaterials, 9*(12), 1735. https://doi.org/10.3390/nano9121735

Wang, Y., Xie, K., Fu, T., & Shi, C. (2019c). Vibration response of a functionally graded graphene nanoplatelet reinforced composite beam under two successive moving masses. *Composite Structures, 209*, 928–939. https://doi.org/10.1016/j.compstruct.2018.11.026

Wattanasakulpong, N., & Bui, T. Q. (2017). Vibration analysis of third-order shear deformable FGM beams with elastic support by Chebyshev collocation method. *International Journal of Structural Stability and Dynamics, 18*(1), 1850071. https://doi.org/10.1142/S021945541850071X

Wattanasakulpong, N., Chaikittiratana, A., & Pornpeerakeat, S. (2018). Chebyshev collocation approach for vibration analysis of functionally graded porous beams based on third-order shear deformation theory. *Acta Mechanica Sinica, 34*(6), 1124–1135. https://doi.org/10.1007/s10409-018-0775-5

Yager, J., Haridas, H., Woods, J. E., & Kontopoulou, M. (2024). Time-dependent mechanical properties and structural behaviour of graphene nanoplatelet-reinforced concrete. *Canadian Journal of Civil Engineering, 52*(5), 700–712. https://doi.org/10.1139/cjce-2023-0182

Yang, B., Kitipornchai, S., Yang, Y. F., & Yang, J. (2017a). 3D thermo-mechanical bending solution of functionally graded graphene reinforced circular and annular plates. *Applied Mathematical Modelling, 49*, 69–86.

https://doi.org/10.1016/j.apm.2017.04.035

Yang, B., & Kitipornchai, S. (2017b). Thermoelastic analysis of functionally graded graphene reinforced rectangular plates based on 3D elasticity. *Meccanica, 52*(10), 2277–2292. https://doi.org/10.1007/s11012-016-0574-3

Yang, B., Mei, J., Chen, D., Yu, F., & Yang, J. (2018a). 3D thermo-mechanical solution of transversely isotropic and functionally graded graphene reinforced elliptical plates. *Composite Structures, 184*, 1040–1048. https://doi.org/10.1016/j.compstruct.2017.10.057

Yang, J., Wu, H., & Kitipornchai, S. (2017). Buckling and post-buckling of functionally graded multilayer graphene platelet-reinforced composite beams. *Composite Structures, 161*, 111–118. https://doi.org/10.1016/j.compstruct.2016.11.048

Yang, Z., Yang, J., Liu, A., & Fu, J. (2018b). Nonlinear in-plane instability of functionally graded multilayer graphene reinforced composite shallow arches. *Composite Structures, 204*, 301–312. https://doi.org/10.1016/j.compstruct.2018.07.085

Zhao, S., Zhao, Z., Yang, Z., Ke, L., Kitipornchai, S., & Yang, J. (2020). Functionally graded graphene reinforced composite structures: A review. *Engineering Structures, 210*, 110339. https://doi.org/10.1016/j.engstruct.2020.110339

Zhao, Z., Feng, C., Wang, Y., & Yang, J. (2017). Bending and vibration analysis of functionally graded trapezoidal nanocomposite plates reinforced with graphene nanoplatelets (GPLs). *Composite Structures, 180*, 799–808. https://doi.org/10.1016/j.compstruct.2017.08.026

Zur, K. K., Arefi, M., Kim, J., & Reddy, J. N. (2020). Free vibration and buckling analyses of magneto-electro-elastic FGM nanoplates based on nonlocal modified higher-order sinusoidal shear deformation theory. *Composites Part B: Engineering, 182*, 107601. https://doi.org/10.1016/j.compositesb.2019.107601